



Full length article

Probing multi-scale mechanical damage in connective tissues using X-ray diffraction

Fabio Bianchi^a, Felix Hofmann^b, Andrew J. Smith^c, Mark S. Thompson^{a,*}^a Institute of Biomedical Engineering (IBME), Department of Engineering Science, University of Oxford, UK^b Department of Engineering Science, University of Oxford, UK^c Diamond Light Source, Didcot, UK

ARTICLE INFO

Article history:

Received 22 March 2016

Received in revised form 8 July 2016

Accepted 17 August 2016

Available online 21 August 2016

Keywords:

Tendon

Collagen

X-ray diffraction

Damage

ABSTRACT

The accumulation of microstructural collagen damage following repetitive loading is linked to painful and debilitating tendon injuries. As a hierarchical, semi-crystalline material, collagen mechanics can be studied using X-ray diffraction. The aim of the study was to describe multi-structural changes in tendon collagen following controlled plastic damage (5% permanent strain). We used small angle X-ray scattering (SAXS) to interrogate the spacing of collagen molecules within a fibril, and wide angle X-ray scattering (WAXS) to measure molecular strains under macroscopic loading.

Simultaneous recordings of SAXS and WAXS patterns, together with whole-tissue strain in physiologically hydrated rat-tail tendons were made during increments of in situ tensile loading. Results showed that while tissue level modulus was unchanged, fibril modulus decreased significantly, and molecular modulus significantly increased. Further, analysis of higher order SAXS peaks suggested structural changes in the gap and overlap regions, possibly localising the damage to molecular cross-links. Our results provide new insight into the fundamental damage processes at work in collagenous tissues and point to new directions for their mitigation and repair.

Statement of Significance

This article reports the first in situ loading synchrotron studies on mechanical damage in collagenous tissues. We provide new insight into the nano- and micro-structural mechanisms of damage processes. Pre-damaged tendons showed differential alteration of moduli at macro, micro and nano-scales as measured using X-ray scattering techniques. Detailed analysis of higher order diffraction peaks suggested damage is localised to molecular cross-links. The results are consistent with previous X-ray scattering studies of tendons and also with recent thermal stability studies on damaged material. Detailed understanding of damage mechanisms is essential in the development of new therapies promoting tissue repair.

© 2016 Acta Materialia Inc. Published by Elsevier Ltd. This is an open access article under the CC BY license (<http://creativecommons.org/licenses/by/4.0/>).

1. Introduction

The mechanical properties of tendons are determined by collagen structure, and microdamage accumulation in the collagen fibrils has been associated with tendon injury [1]. Tendon injury and pathology are painful and disabling, and understanding the mechanisms underlying collagen damage can lead to novel strategies to diagnose and prevent injury, and facilitate regeneration. This requires comprehensive knowledge of collagen mechanics, cell-matrix interactions, and of the structural and biochemical response

to loading and damage accumulation. [2] Tendons are composite materials, where collagen accounts for 86% of dry mass [3]. Three alpha chains, consisting of 1056, 0.29-nm spaced amino-acid residues arranged in a Gly-X-Y repeat pattern, combine to form 300 nm long triple-helical collagen molecules. These assemble into five-staggered microfibrils with a characteristic 67 nm D-period, forming the base crystallographic unit of collagen; as described by the consensus axial packing model, formulated by Hodge and Petruska in 1964 [4,5]. The fibrillar D-period is made up of a gap region of lower electron density, and an overlap region, where laterally adjoining, non-helical molecule terminals are cross-linked, stabilising the structure [6,7]. Interlaced microfibrils form fibrils, which combine with a proteoglycan-rich matrix, that maintains

* Corresponding author.

E-mail address: mark.thompson@eng.ox.ac.uk (M.S. Thompson).

physiological hydration, to form fibres [8]. Tenocytes, specialised fibroblastic cells of elongated cytoplasm morphology, sparsely populate the tendon, and maintain homeostasis of the tissue. [2] Due to this complex hierarchical organisation, strain partitioning between structural levels and damage mechanisms in tendons are not well understood. Whole tendon deformation results from fibrillar straining and intra-fibrillar matrix deformation. Fibrillar straining, in turn, is a compound effect of molecular deformation and molecular rearrangement [8,9]. Micro-damage accumulation at small length scales may lead to pain and loss of functionality and ultimately macroscopic failure [10].

Deformation mechanisms and mechanical properties at the nanoscale can be probed using in situ loading experiments with X-ray diffraction, due to the quasi-crystalline organisation of collagen at fibril and molecular level. Small angle diffraction (SAXS) has been used to measure the 67 nm D-period between repeat units in fibrils [6,11], while wide-angle diffraction (WAXS) can measure the 0.29 nm intra-amino acid spacing along the molecular axis [12]. Fibrillar and molecular strain can be estimated from the shifting of diffraction peaks during in situ loading [9]. Further analysis of the diffraction patterns can provide structural information: The ratio of integrated intensities of the second and third order SAXS peaks is directly correlated to the ratio of the overlap region length to that of the whole D-period [9,13], capturing structural changes due to load. Furthermore, lateral packing and fibril distribution affect damage mechanisms, and have been probed in recent years using X-ray ptychography [14]. Previous X-ray diffraction (XRD) investigations of non-physiological damage to fibrillar collagen through dehydration and heating have shown changes to lateral packing tightening and fibrillar

D-period shrinking to 64 nm, resulting in a loss of gap-overlap periodicity and a shearing of molecular packing [6,15]. However physiological mechanical damage mechanisms have not been investigated using these techniques. The aim of this investigation is to describe collagen material property changes at three length scales following mechanical damage applied under physiological conditions, and to suggest potential underlying deformation and damage mechanisms. This was achieved using in situ mechanical loading and X-ray scattering to compute the multi-scale mechanical properties at each hierarchical level, to investigate the relationship between these properties and pre-applied mechanical damage.

2. Materials and methods

2.1. Tendon harvesting

Tendons were harvested from 300 to 350 g (10–12 week old), male Sprague–Dawley rats, sacrificed by cervical dislocation for an unrelated study, by adapting the method described in [16]. Briefly, individual fascicles were separated, and selected based on diameter ($0.22 \text{ mm} \pm 0.05 \text{ mm}$, measured using an optical micrometer (Keyence, Milton Keynes, UK; precision $1 \times 10^{-5} \text{ mm}$). A tendon sub-population was pre-damaged, and all samples were fixed to neodymium magnets (8 mm diameter by 10 mm) using epoxy putty, and frozen at -20 in Phosphate Buffered Saline (PBS, Gibco, UK) until use, to not alter the mechanical properties of the tendons [13]. Black ink marks (see arrows in Fig. 1(d)) were made on all samples, for optical measurement of whole tissue strain.

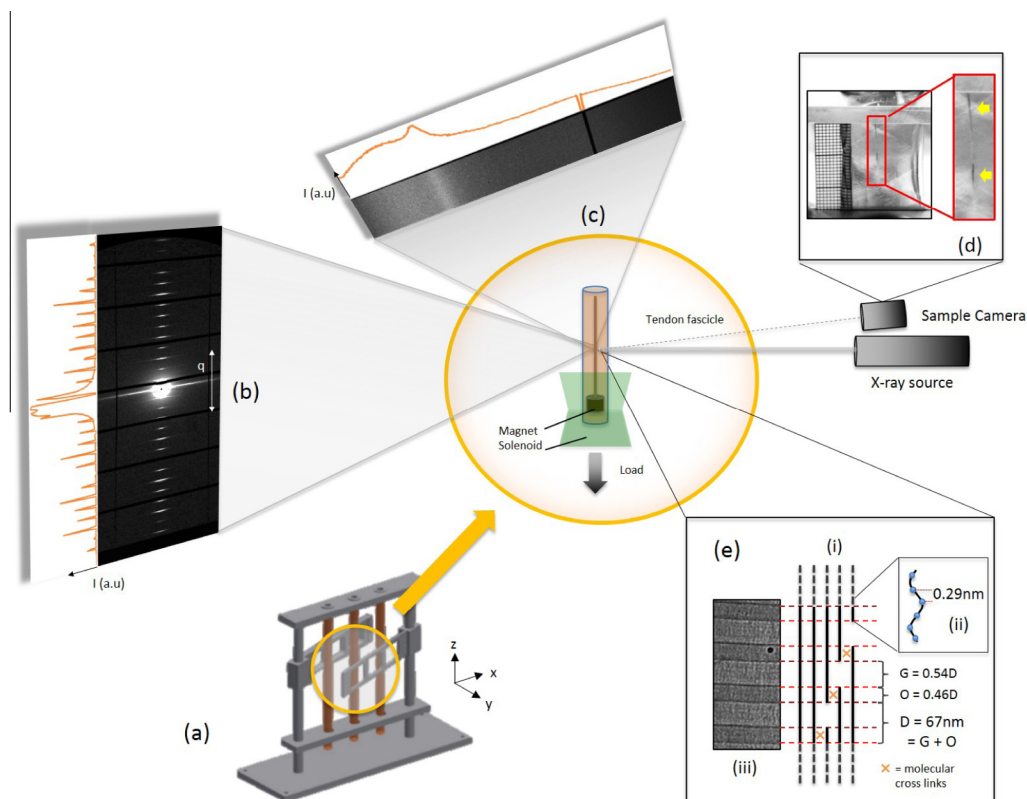


Fig. 1. Experimental setup and data acquisition. (a) Sample rig, placed on precision linear table and allowing remote load application to the fully hydrated tendon. (b) SAXS signal detector output, showing collagen diffraction peaks (up to 12th order), where distance between peaks corresponds to 67 nm D-period arising from the five-staggered arrangement within fibrils. (c) WAXS detector output, showing single peak corresponding to the 0.29 nm intra amino-acid spacing along alpha chain. (d) High definition camera collecting images to measure macroscopic tissue strain. Yellow Arrows indicate permanent marks (e) Collagen nanostructure (i) Arrangement of molecules within fibrils, showing the characteristic 67 nm D-period, which is the sum of gap and overlap regions. (ii) Single alpha-chain with amino-acid residues (iii) electron micrograph of fibril, showing gap and overlap contrast due to the square-wave variation of electron density along the fibril.

2.2. Pre-damage application

Tendons ($n = 6$) were pre-damaged using a bench top uniaxial strain machine (Bose Electroforce, Eden Prairie, MN), by applying a continuous 10 MPa load for 500 s. Samples were then placed in PBS for 2 min, and damage quantified by manual measurement of permanent change in length between two ink marks. A length change greater than 5% was selected as the damage threshold. Multiphoton microscopy of other samples damaged to this level confirmed microstructural changes as described previously [17]. This level of damage is physiologically relevant for induction of tendinopathy in animal models of disease [17].

2.3. In situ loading

Tendons were loaded in situ using an electromagnetic loading setup, consisting of a remotely operated, current-controlled solenoid, applying forces up to 0.5 N. Samples were placed in PBS-filled Kapton tubing, sealed using Polydimethylsiloxane (PDMS, Corning, UK) to maintain hydration, and held by a custom-built experimental rig, designed to fit within the sample space of the I22 beamline at the Diamond Light Source, UK, and mounted on a linear translation table for positioning (Fig. 1(a)). Each magnet, weighing 6.1 g, produced a 0.06 N tare load when the solenoid was inactive.

2.4. X-ray diffractometry

Diffraction experiments were carried out at beamline I22, Diamond Light Source, UK. The X-ray beam was coarsely focused to $90 \times 110 \mu\text{m}^2$ (full width at half maximum), with the largest dimension parallel to the sample axis (z-direction in Fig. 1(a)). The optical design of I22 typically generates beamsizes at the sample of $300 \times 100 \mu\text{m}^2$, horizontal \times vertical (Full width at half maximum) by directly reimaging the X-ray source in a 1:1 focussing arrangement. For these experiments the beamsizes were reduced to $110 \times 90 \mu\text{m}^2$, horizontal \times vertical, using collimating slits with an attendant loss of flux. This represents a compromise between minimising beamsizes and maximising flux whilst maintaining the naturally low divergence of I22 ($80 \times 50 \mu\text{rad}$, horizontal \times vertical) essential for high quality SAXS data collection. Smaller beamsizes without loss of flux could be achieved through the use of additional focussing optics, however the increased demagnification here would be offset by increased beam divergence that would negatively impact data quality. A photon energy of

$12.4012 \pm 0.0014 \text{ keV}$ was selected ($\frac{\Delta E}{E} = 1.12 \times 10^{-4}$), corresponding to an X-ray wavelength of $0.0997 \pm 1.066 \times 10^{-5} \text{ nm}$. SAXS data was collected over a q range of $0.0025 - 0.15 \text{ \AA}^{-1}$, and over an azimuthal range of 360° using a 2D Pilatus P3-2 M detector (DECTRIS, Switzerland) placed 9 m from the sample and with an exposure time of 5 s. WAXS data was collected for a 2θ range of $16 - 50^\circ$ on a 1D Pilatus P300k-W detector (DECTRIS, Switzerland), for 5 s at every loading point (Fig. 1(b) and (c)). A high definition camera placed above the beamline exit, triggered by the beamline software, and focused on the sample was used to record sample images for macro strain computation by image correlation (Fig. 1(e)).

2.5. X-ray diffraction pattern analysis

SAXS diffraction patterns, showing distinct meridional peaks up to the 12th order were converted from polar to Cartesian coordinates, using dried chicken collagen as a calibration reference (Fig. 1(b)). Hence, a radial line profile for the 12 peaks was extracted, using both upper and lower reflections. Gaussian curves fitted to the peaks were used to compute peak position, full width at half maximum (FWHM) and integrated intensity. WAXS diffraction patterns were collected in 1D due to detector geometry. Calibration of the detector geometry was performed using a CeO_2 standard. A single peak was extracted by fitting a Gaussian curve to the line profile obtained by averaging the detector output in the y direction. Peak position, FWHM and integrated intensities were calculated.

2.6. Sample camera tissue strain

High definition, 1292×962 pixel images of samples taken at each load point were used to compute tissue strain with a custom-written Matlab digital image correlation routine.

2.7. Statistical analysis

Statistical analysis (paired, two-tailed t -tests) was carried out using Graphpad PRISM. $p < 0.05$ indicated statistical significance of results (95% confidence interval).

2.8. Ethics approval

All tissues were harvested from rats sacrificed for unrelated experiments, and thus no ethical approval was required.

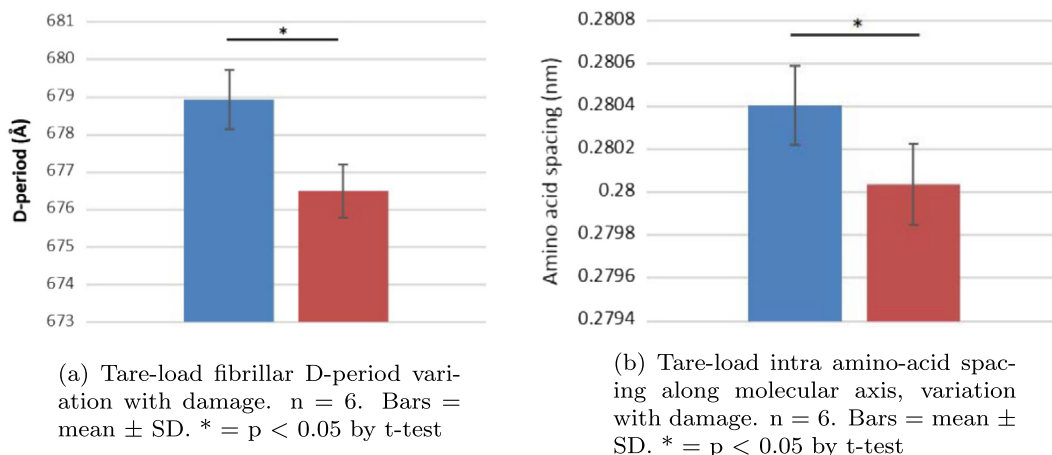


Fig. 2. Fibril D-period and amino-acid spacing variation with damage. Blue = undamaged, Red = pre-damaged. (For interpretation of the references to colour in this figure legend, the reader is referred to the web version of this article.)

3. Results and discussion

3.1. D-period variation with damage

Comparison between damaged ($N = 6$) and undamaged ($N = 6$) populations tare load D-period (i.e. before solenoid activation) indicates a significant decrease in both fibrillar D-period and intra-amino-acid spacing with damage application (Fig. 2).

Significant shortening of intra amino-acid spacing and shortening of fibrillar D-period (Fig. 2a and b) have been shown to be related to X-ray radiation damage [13] and dehydration [18]. Due to minimal exposure to X-rays, and continuous sample hydration by immersion in PBS, neither mechanism could explain the change in D-periods observed here. This was verified by comparison of measured D-period before and after a full scan, showing no significant change, on average, in D-period (data not shown).

3.2. Strain partitioning and stiffness changes with damage

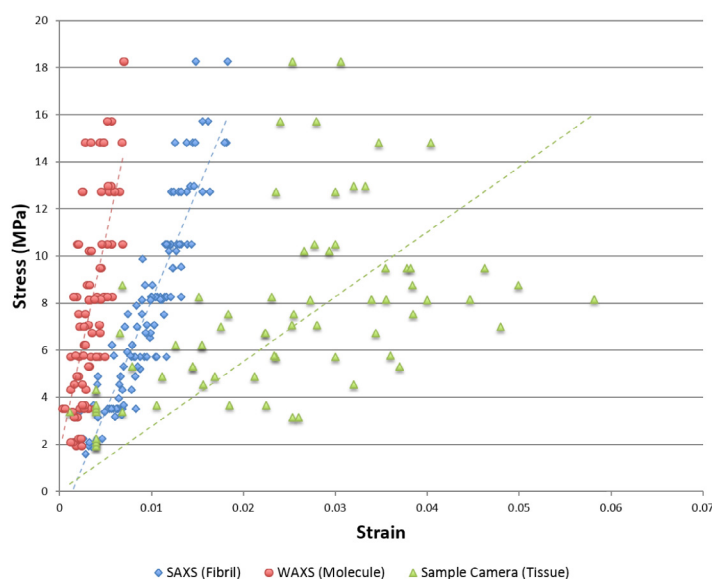
During fascicle elongation, the strain induced by applied stress is distributed between the collagen fibrils and the interfibrillar

ground substance [8]. The fibril strain is in itself a compound effect of an affine elongation of the collagen molecules, and a rearrangement of the molecular structure within the five-staggered unit [9]. Here, we can evaluate how this partitioning of strain is affected by deformation damage, by simultaneous collection of WAXS, SAXS and Macroscopic high definition sample camera data.

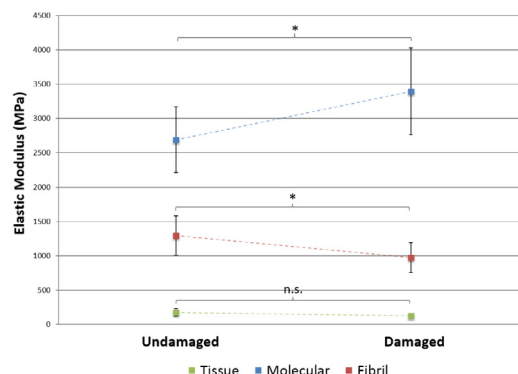
From peak positions of SAXS and WAXS patterns and from macro images, straining of the characteristic measured length was calculated as:

$$\epsilon_X = \frac{X - X_0}{X_0} \quad (1)$$

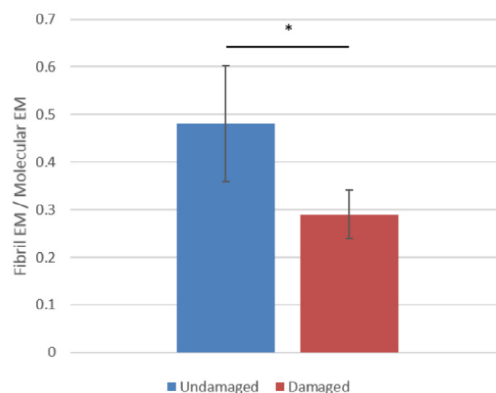
where X_0 denotes the average characteristic length (D-period for SAXS, amino-acid spacing for WAXS, macro length for sample camera) of the unloaded sample and X denotes the characteristic length calculated from the loaded diffraction pattern. X_0 for SAXS and WAXS was calculated as an average of measurements taken twice at 5 positions along the tendons axis, for $n = 3$ unloaded tendons. Unloaded D-period for SAXS was computed as $674.5 \text{ \AA} \pm 0.07\%$. Unloaded intra amino-acid spacing from WAXS was calculated as $2.798 \text{ \AA} \pm 0.09\%$.



(a) Stress-Strain curves for all measurement levels and damage levels, showing partitioning of strain between tissue, fibril and molecule



(b) Fibril loading modulus (SAXS) and Molecule loading modulus (WAXS) as a function of damage level. Mean \pm SD. * = $p < 0.05$ by t-test



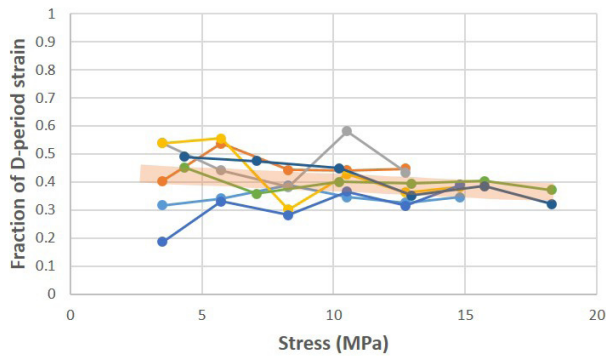
(c) Ratio of fibril loading modulus to molecule loading modulus, in relation to damage level. * = $p < 0.05$ by t-test. $n = 6$. Mean \pm SD

Fig. 3. Stress-strain curves from in situ tensile loading of tendon fascicles probed by X-ray diffraction, and loading modulus relation to damage.

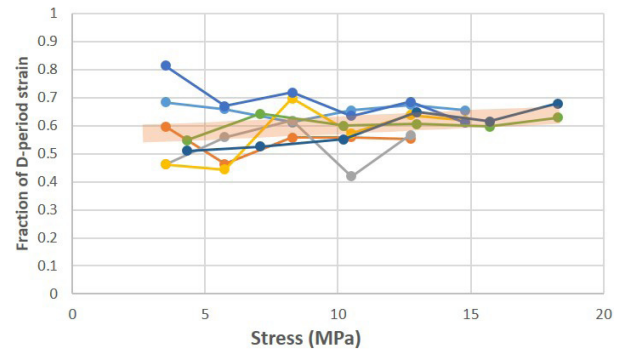
3.2.1. Loading moduli of fibril, molecule and tissue

Strains measured at the three length scales probed were plotted against stress. Stress calculations assumed tight lateral packing of molecules and fibrils. Stress–strain curves for molecules and fibrils

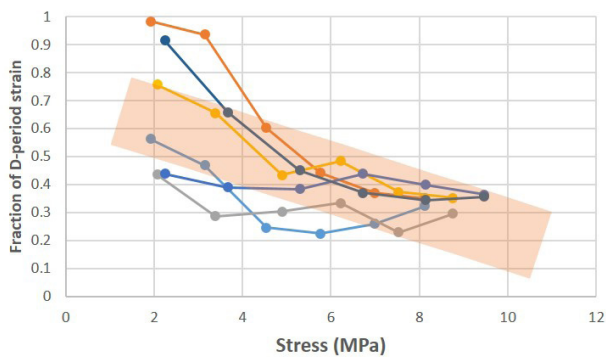
show linear increasing trends for all samples (Fig. 3a), confirming the elastic nature of the material, allowing loading moduli to be calculated from the curve slopes. Fig. 3a confirms strain partitioning at the three structural levels: molecular elongation is lower



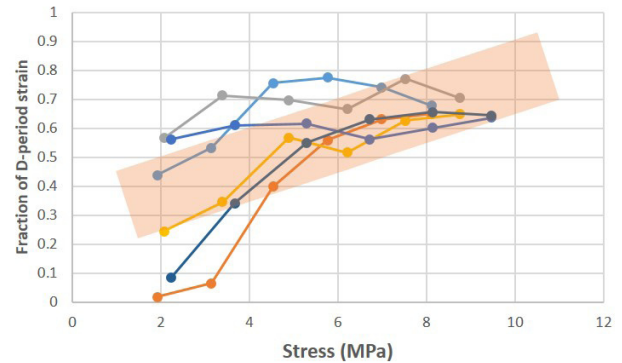
(a) Fraction of fibril (D-period) strain due to molecular elongation. Undamaged samples



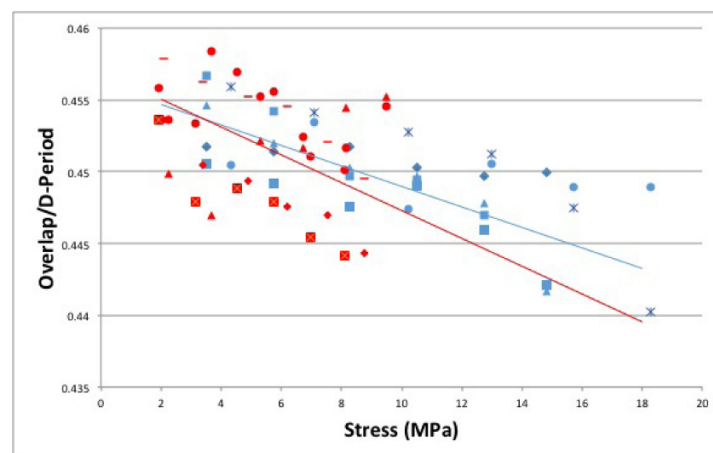
(b) Fraction of fibril (D-period) strain due to molecular rearrangements. Undamaged samples



(c) Fraction of fibril (D-period) strain due to molecular elongation. Damaged samples



(d) Fraction of fibril (D-period) strain due to molecular rearrangements. Damaged samples



(e) Ratio of Overlap to D-Period as a function of stress. Blue = undamaged, Red = Damaged

Fig. 4. Molecular elongation and rearrangement contributions to fibril deformation. Red bars = average slope of data sets from corresponding condition. Red bar thickness represents deviation of slopes (thicker bar = higher deviation, a.u.). (For interpretation of the references to colour in this figure legend, the reader is referred to the web version of this article.)

than that of fibrils, which in turn is lower than whole tissue elongation. This confirms additional mechanisms involved during loading of tendon samples, with a rearrangement of collagen molecules accounting for the additional strain measured in fibrils, and ground substance deformation and fibril superstructure rearrangement contributing to higher strains measured in the whole tissue sample [8]. Studies of cross-link deficient tendons have shown an increase in this effect, indicating the cross-link locations as the areas which are deformed during straining [19].

Tissue-level stiffness was not significantly affected by pre-applied damage (Fig. 3b). Mean fibril loading modulus, decreased significantly ($p < 0.05$) from 1300 to 900 MPa with pre-applied damage (Fig. 3b). Conversely, average molecular loading modulus significantly ($p < 0.05$) increased from 2690 to 3395 MPa with damage. This divergent behavior indicates permanent changes to the structural organisation of the tissue following damage application. Qualitatively, molecular stiffening observed might be explained by a change in triple helix geometry, as reported for mechanically overloaded tendon collagen, which denatures with load application. Previous studies on overloaded collagen fibrils showed a reduction in enthalpy of denaturation, and proposed that the collagen molecules were uncoiled into a stable denatured state, consistent with our observations [20]. This may reduce axial mobility of neighboring amino-acids and thus reducing the increase in intra-amino-acid spacing as load is applied [21]. The loss of stiffness at the fibril level implies ulterior deformation mechanisms in fibril straining, not limited to affine deformation from triple helix straining [19,22].

3.3. Damage alters tendon deformation modalities

Combining simultaneous WAXS and SAXS data, the contributions of deformation modes to the overall deformation of the tissue were calculated. Assuming fibril elongation to be an additive effect of an affine molecular stretch and molecular rearrangements, then:

$$E_D = E_M + M \quad (2)$$

where E_D is the elongation (nm) at the fibrillar D-period level, E_M is the elongation of intra-amino-acid spacing along a molecule (nm), and M includes all molecular rearrangement effects. Hence, overall stretch of the fibril D-period can be described by:

$$(1 + \epsilon_D) * D_0 = D_0(1 + \epsilon_m) + M \quad (3)$$

where D_0 is the fibril D-period in unloaded state and ϵ_m is the strain at the molecular level.

From Eq. 3, using WAXS and SAXS data, undamaged samples qualitatively showed a more uniform partitioning of D-period deformation between molecular elongation and rearrangement, with an average decrease in elongation and increase in rearrangements with stress (Fig. 4a and b). Molecular elongation decreased rapidly in damaged samples (Fig. 4c), with rearrangements conversely increasing (Fig. 4d), apparent at low stresses (<6 MPa). In both groups, molecular elongation converged to approximately 0.38% of D-period strain at high stresses.

3.4. Damage causes changes in structure

Changes in the molecular arrangement, caused by sliding of laterally and axially adjacent molecules, cause a variation in the ratio of the overlap region to the total D-period. These changes account for the higher straining of fibrillar D-period compared to only an affine molecular deformation.

Assuming the electron density along a fibril is described by a square function with a period of 67 nm, having a low period (gap) of 0.54D and a high period (overlap) of 0.46D, a variation in gap and overlap would result in a change in the relative

integrated intensities of successive SAXS peaks [23,9]. This can be described as:

$$\frac{I_{n+1}}{I_n} = \left(\frac{n}{n+1} \right)^2 \left[\frac{\sin((n+1)\pi[O/D])}{\sin(n\pi[O/D])} \right]^2 \quad (4)$$

where n is the peak order, O is the overlap length, and D is the D-period length. Qualitative analysis of O/D values plotted against stress indicates a steeper average decrease for damaged samples compared to undamaged samples (Fig. 4e). Since the D-period has been shown to decrease with damage (Fig. 2a), this effect must be due to the overlap region shrinking faster in damaged samples. This region corresponds to the location of cross-links between terminals of laterally adjacent collagen molecules within fibrils, and an increased deformation as a result of applied stress may implicate cross-link damage as the location of tensile damage. In artificially-induced hyper-cross linking, the opposite effect is observed [13], suggesting that damage accumulation decreases cumulative cross-linking strength.

3.5. Limitations of experimental method and analysis

To further understand the mechanisms of damage in collagenous connective tissues, the ability to probe lateral packing of fibrils and helical arrangement of molecules simultaneously would allow for a more complete appraisal of structural changes with damage, by measuring triple helix pitch and fibril helical characteristics [24,5,25].

4. Conclusions

Understanding collagen damage at the nanoscale is key to preventing injury from accumulated micro-damage, as well as to develop strategies for encouraging healing. X-ray diffraction allows us to probe biological collagenous tissues at the nanoscale. By performing in situ mechanical loading it is possible to probe the mechanical properties at various scales within the collagenous superstructure. Simultaneous data collection is key to studying the molecular, fibrillar and tissue behaviour under load, and exploring the relationship between these three structural levels.

Here, we focus on the effects of mechanical damage induced by tensile elongation on the mechanical properties of rat tail tendons at two scales: the fibril and the molecular scales. We show a significant decrease in both fibril D-period and molecular intra-amino acid spacing as a result of applied damage, which is indicative of damage mechanisms at both scales. We have shown significant loss of fibril level stiffness and significant increase of stiffness at the molecule level following damage, indicating distinct mechanisms at the two levels. The overlap region of the fibrillar D-period exhibits a faster reduction in length in damaged samples than the gap region, indicative of potential damage being localised here, where laterally adjacent collagen molecules are cross-linked. This is consistent with the observed inhomogeneous partitioning of D-period strain between molecular elongation and rearrangements observed in damaged samples, once again indicating damage localised where the mechanisms allowing molecules to move relative to one another are found.

Acknowledgements

This work was supported by the Rosetrees Trust (award M186-F1) for materials and EPSRC (DTP Programme studentship funding). We acknowledge Diamond Light Source for time on beamline I22 under proposal SM10601-1.

References

- [1] A. Neviaser, N. Andarawis-Puri, E. Flatow, Basic mechanisms of tendon fatigue damage, *J. Shoulder Elbow Surg.* 21 (2) (2012) 158–163.
- [2] P. Sharma, N. Maffulli, Tendon injury and tendinopathy: healing and repair, *J. Bone Joint Surg. Am.* 87 (1) (2005) 187–202.
- [3] M.E. Nimni, Collagen: structure, function, and metabolism in normal and fibrotic tissues, *Semin. Arthritis Rheum.* 13 (1983) 1–86.
- [4] J.A. Petruska, A.J. Hodge, A subunit model for the tropocollagen macromolecule, *Proc. Natl. Acad. Sci. U.S.A.* 51 (1964) 871–876.
- [5] T.J. Wess, A.P. Hammersley, L. Wess, A. Miller, Molecular packing of type I collagen in tendon, *J. Mol. Biol.* 275 (2) (1998) 255–267.
- [6] J.P. Orgel, T.J. Wess, A. Miller, The in situ conformation and axial location of the intermolecular cross-linked non-helical telopeptides of type I collagen, *Structure* 8 (2) (2000) 137–142.
- [7] T.J. Wess, D.E. Cairns, Nanoarchitectures of the animal extracellular matrix: opportunities for synchrotron radiation studies on collagen and fibrillin, *J. Synchrotron. Radiat.* 12 (Pt 6) (2005) 751–757.
- [8] P. Fratzl, K. Misof, I. Zizak, G. Rapp, H. Amenitsch, S. Bernstorff, Fibrillar structure and mechanical properties of collagen, *J. Struct. Biol.* 122 (1–2) (1998) 119–122.
- [9] N. Sasaki, S. Odajima, Elongation mechanism of collagen fibrils and force-strain relations of tendon at each level of structural hierarchy, *J. Biomech.* 29 (1996) 1131–1136.
- [10] M.S. Thompson, Tendon mechanobiology: experimental models require mathematical underpinning, *Bull. Math. Biol.* 75 (2013) 1238–1254.
- [11] P.M. Cowan, A. North, J.T. Randall, X-ray diffraction studies of collagen fibres, *Symposia of the Society for Experimental Biology*, vol. 9, 1955, pp. 115–126. bcin.ca.
- [12] N. Sasaki, S. Odajima, Stress-strain curve and young's modulus of a collagen molecule as determined by the X-ray diffraction technique, *J. Biomech.* 29 (1996) 655–658.
- [13] G. Fessel, Y. Li, V. Diederich, M. Guizar-Sicairos, P. Schneider, D.R. Sell, V.M. Monnier, J.G. Snedeker, Advanced glycation end-products reduce collagen molecular sliding to affect collagen fibril damage mechanisms but not stiffness, *PLoS One* 9 (11) (2014) e110948.
- [14] F. Berenguer, R.J. Bean, L. Bozec, J. Vila-Comamala, F. Zhang, C.M. Kewish, O. Bunk, J.M. Rodenburg, I.K. Robinson, Coherent X-ray imaging of collagen fibril distributions within intact tendons, *Biophys. J.* 106 (2) (2014) 459–466.
- [15] T.J. Wess, J.P. Orgel, Changes in collagen structure: drying, dehydrothermal treatment and relation to long term deterioration, *Thermochim. Acta* 365 (1–2) (2000) 119–128.
- [16] A. Bruneau, N. Champagne, P. Cousineau-Pelletier, G. Parent, E. Langelier, Preparation of rat tail tendons for biomechanical and mechanobiological studies, *J. Vis. Exp.* (2010).
- [17] D.T. Fung, V.M. Wang, N. Andarawis-Puri, J. Basta-Pljakic, Y. Li, D.M. Laudier, H. B. Sun, K.J. Jepsen, M.B. Schaffler, E.L. Flatow, Early response to tendon fatigue damage accumulation in a novel in vivo model, *J. Biomech.* 43 (2) (2010) 274–279.
- [18] R.I. Price, S. Lees, D.A. Kirschner, X-ray diffraction analysis of tendon collagen at ambient and cryogenic temperatures: role of hydration, *Int. J. Biol. Macromol.* 20 (1997) 23–33.
- [19] R. Puxkandl, I. Zizak, O. Paris, J. Keckes, W. Tesch, S. Bernstorff, P. Purslow, P. Fratzl, Viscoelastic properties of collagen: synchrotron radiation investigations and structural model, *Philos. Trans. R. Soc. London B Biol. Sci.* 357 (1418) (2002) 191–197.
- [20] S.P. Veres, J.M. Harrison, J.M. Lee, Mechanically overloading collagen fibrils uncoils collagen molecules, placing them in a stable, denatured state, *Matrix Biol.* 33 (2014) 54–59.
- [21] S.P. Veres, J.M. Lee, Designed to fail: a novel mode of collagen fibril disruption and its relevance to tissue toughness, *Biophys. J.* 102 (12) (2012) 2876–2884.
- [22] E. Mosler, W. Folkhard, E. Knorz, H. Nemetschek-Gansler, T. Nemetschek, M. H. Koch, Stress-induced molecular rearrangement in tendon collagen, *J. Mol. Biol.* 182 (1985) 589–596.
- [23] A. Bigi, A.M. Fichera, N. Roveri, M.H.J. Koch, Structural modifications of Air-Dried tendon collagen on heating, *Int. J. Biol. Macromol.* 9 (1987) 176–180.
- [24] R.D. Fraser, T.P. MacRae, A. Miller, E. Suzuki, Molecular conformation and packing in collagen fibrils, *J. Mol. Biol.* 167 (2) (1983) 497–521.
- [25] A. Masic, L. Bertinetti, R. Schuetz, S.-W. Chang, T.H. Metzger, M.J. Buehler, P. Fratzl, Osmotic pressure induced tensile forces in tendon collagen, *Nat. Commun.* 6 (2015) 5942.